Myosin-II mediated traction forces evoke localized Piezo1 Ca^{2+} flickers

Kyle L. Ellefsen[† 1], Alice Chang[† 2], Jamison L. Nourse[† 3,6], Jesse R. Holt[† 3,6], Janahan Arulmoli [4,6], Armen Mekhdjian [2], Hamid Abuwarda [3,6], Francesco Tombola [3], Lisa A. Flanagan [4,5,6], Alexander R. Dunn [2], Ian Parker [1,3], Medha M. Pathak [3,6,7,*]

[1] Department of Neurobiology & Behavior, UC Irvine, Irvine, CA 92697.
[2] Department of Chemical Engineering, Stanford University, Stanford, CA 94305.
[3] Department of Physiology & Biophysics, UC Irvine, Irvine, CA 92697.
[4] Department of Biomedical Engineering, UC Irvine, Irvine, CA 92697.
[5] Department of Neurology, UC Irvine, Irvine, CA 92697.
[6] Sue and Bill Gross Stem Cell Research Center, UC Irvine, Irvine, CA 92697.
[7] Center for Complex Biological Systems, UC Irvine, Irvine, CA 92697.

† Equal contribution
* Correspondence: medhap@uci.edu

ABSTRACT

Piezo channels transduce mechanical stimuli into electrical and chemical signals to powerfully influence development, homeostasis, and regeneration. Given their location in the plasma membrane, Piezo channels are positioned to transduce both external forces and internal forces generated by cells. While much is known about how Piezo1 responds to external forces, its response to internal, cell-generated forces vital for cellular and organismal physiology is poorly understood. Here, using direct measurements of endogenous Piezo1 activity and traction forces in native cellular conditions, we show that actomyosin-based cellular traction forces generate spatially-restricted Ca^{2+} flickers in the absence of dynamic, externally-applied mechanical forces. Although Piezo1 channels diffuse readily in the plasma membrane and are widely distributed across the cell, their flicker activity is enriched in regions proximal to force-producing adhesions. The mechanical force that activates Piezo1 arises from Myosin II phosphorylation by Myosin Light Chain Kinase. We propose that Piezo1 Ca^{2+} flickers allow spatial segregation of mechanotransduction events, and that diffusion allows channel molecules to efficiently respond to transient, local mechanical stimuli.

Keywords: Piezo1, traction forces, micropatterned cells, molecular tension sensor, Piezo1 diffusion, Ca^{2+} signaling, Ca^{2+} flickers, Myosin II, MLCK, ROCK

INTRODUCTION

Cells have the ability to detect and generate mechanical forces, and to integrate this mechanical information with genetic and chemical cues to shape organismal morphology, growth, and homeostasis. Mechanical forces are transduced into biochemical signals by specialized proteins. Among these, mechanically-activated ion channels provide unique features: sub-millisecond response to mechanical stimuli, high sensitivity, large dynamic range, spatial coding of mechanical stimuli, and the ability to temporally filter repetitive stimuli [1].

Piezo channels were recently identified as a new family of excitatory mechanically-activated channels [2,3]. Due to their permeability to Ca^{2+} and other cations, Piezo channel activity generates chemical as well as electrical signals in response to mechanical stimuli, allowing them to regulate a wide variety of cellular processes. Indeed, Piezo1 has emerged as an important player in vascular development [4,5], stem cell differentiation [6,7], epithelial homeostasis [8], bladder mechanosensation [9], erythrocyte volume regulation [10], cell migration [11–13], vascular smooth muscle remodeling [14], cartilage mechanics [15,16], blood pressure regulation [17] and exercise physiology [18]. The global knockout of Piezo1 is embryonic lethal [5], and mutations in the channel have been linked to diseases such as dehydrated hereditary stomatocytosis [19–22], colorectal adenomatous polyposis [23], generalized lymphatic dysplasia [24,25] and malarial parasite infection [26]. Thus, understanding how Piezo1 functions is critical for deciphering its diverse physiological roles.

Studies on Piezo1 have largely focused on transduction of dynamic mechanical forces from outside the cell to inside the cell, for instance, through application of a poking stimulus, membrane stretch, shear flow, osmotic stress and displacement of the substrate [2,4,27–30]. However, cells also actively generate intracellular mechanical forces that serve as critical regulators of cell signaling and function [31]. As an integral membrane protein, Piezo1 is situated to respond to both intracellular and extracellular mechanical forces. Most studies of Piezo1 activation have utilized patch clamp assays that, by their design, evaluate Piezo1 response to externally-applied mechanical stimuli. Moreover, patch clamp measurements drastically affect the native environment of the channel, making them incompatible for studying the response of Piezo1 to cell-generated forces. In whole-cell patch clamp, cellular contents are dialyzed by the large reservoir of solution in the patch pipette, confounding the study of channel activation and modulation by the cytoskeleton and by soluble intracellular molecules. In cell-attached patch clamp, the intracellular contents are retained, but the gigaseal connection between the membrane and glass pipette exerts intense mechanical stress on the membrane patch [32]. This is sufficient to drive a large fraction of Piezo1 channels into inactivation [33], resulting in a higher activation threshold compared to physiological conditions.

An alternative, non-perturbing method to monitor activation of Piezo1 channels involves imaging Ca^{2+} flux through the channel rather than electrophysiological measurements of ionic current [7,34]. Using this approach in human neural stem/progenitor cells (hNSPCs), we previously found that endogenous Piezo1 underlies discrete, local, and transient Ca^{2+} microdomains or "flickers" in the absence of dynamic externally-applied mechanical forces. This activity, which requires the action of Myosin II motors, underlies the mechanosensitive lineage choice of hNSPCs during differentiation [7]. Here we image Piezo1 flickers at submicron-scale spatial resolution and millisecond-scale temporal resolution. In conjunction with direct observation of Piezo1 channels in live cells and techniques to manipulate [35,36] and measure cell-generated actomyosin forces [37–39], this approach allows us to examine the spatial regulation of Piezo1 by traction forces. We find that although Piezo1 channels appear to diffuse readily in the plasma membrane and are widely distributed across the cell, flicker activity is enriched in the vicinity of force-producing adhesions. Moreover, Piezo1 flickers are triggered by activation of Myosin II through phosphorylation by Myosin Light Chain Kinase (MLCK) but not by Rho-associated protein kinase (ROCK). In light of recent evidence demonstrating that membrane tension gates Piezo1 [27,28,33], our studies suggest that cellular traction forces generate local increases in membrane tension that activates Piezo1 within spatial microdomains. We further propose that Piezo1 channel mobility allows a small number of channels to explore large areas of the cell membrane, and hence respond to both unpredictable external forces as well as to hotspots of cell-generated traction forces.

RESULTS

Piezo1 generates Ca^{2+} flickers

We previously reported Ca^{2+} flickers observed by Total Internal Reflection Fluorescence Microscopy (TIRFM) imaging of hNSPCs in the absence of external mechanical stimulation [7]. These Ca^{2+}

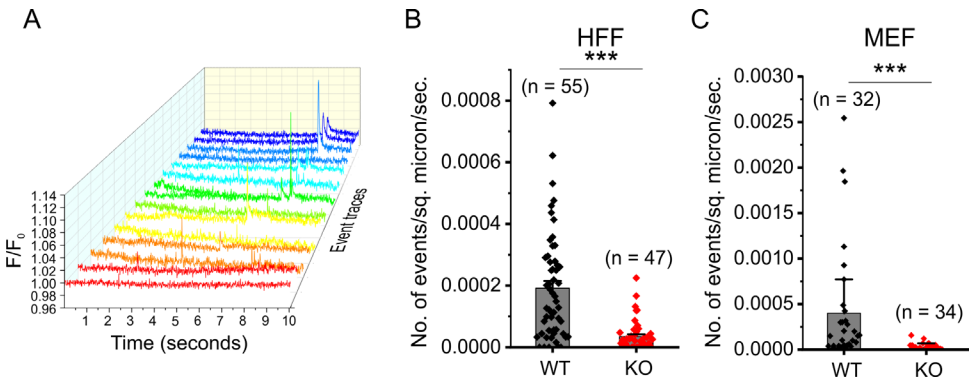

Figure 1. Piezo1 channels generate Ca^{2+} flickers. A. Representative Ca^{2+} flickers recorded from HFF cells. Traces show fluorescence ratio changes ($\Delta F/F_0$) from multiple regions of interest, plotted over time and in different colors for clarity. **B.** Frequency of Ca^{2+} flickers in Wildtype HFFs and in Piezo1-knockout HFFs. Bars denote mean ± sem and each point represents flicker frequency in an individual video. **C.** Frequency of Ca^{2+} flickers in Piezo1-knockout MEFs and in Wildtype MEFs derived from littermate embryos. n values for panels B and C denote number of videos from three different experiments. *** denotes $p < 0.001$ by Kolmogorov-Smirnov test. See also Fig. S1.

flickers were substantially reduced following siRNA-mediated Piezo1 knockdown, indicating that they were produced by Piezo1 activity [7]. Here we extend the finding to Human Foreskin Fibroblasts (HFFs) and to Mouse Embryonic Fibroblasts (MEFs). Like hNSPCs, both cell types showed Ca^{2+} events in the absence of external mechanical stimulation (Fig. 1). A CRISPR knockout of the Piezo1 gene in HFFs showed 82% reduction in Ca^{2+} flickers compared to wild-type cells (Fig. 1B, Movie M1). Residual Ca^{2+} events in Piezo1 KO HFFs persisted in the absence of extracellular Ca^{2+} (Fig. S1), suggesting that these are produced by liberation of Ca^{2+} from intracellular stores. MEFs derived from constitutive Piezo1 knockout mice [5] showed 94% lower occurrence of Ca^{2+} flickers compared to MEFs from wild-type littermate embryos (Fig. 1C, Movie M2). Together, we provide evidence that a large majority of Ca^{2+} flickers in hNSPCs [7], HFFs, and MEFs derive from Piezo1 activity.

Super-resolution localization of Ca^{2+} flickers

To examine the spatial relationship of Piezo1 flickers relative to hotspots of traction forces, we developed a technique for automated localization of Piezo1 flickers at super-resolution levels (Fig. 2). This approach is an improved version of our algorithm for automated detection and quantitation of local Ca^{2+} signals [40], implemented as a plugin for the general purpose image processing software Flika (http://flika-org.github.io). The algorithm uses a clustering method [41] to group suprathreshold pixels into Ca^{2+} events, improving the unbiased detection and segregation of signals (see Methods for further details).

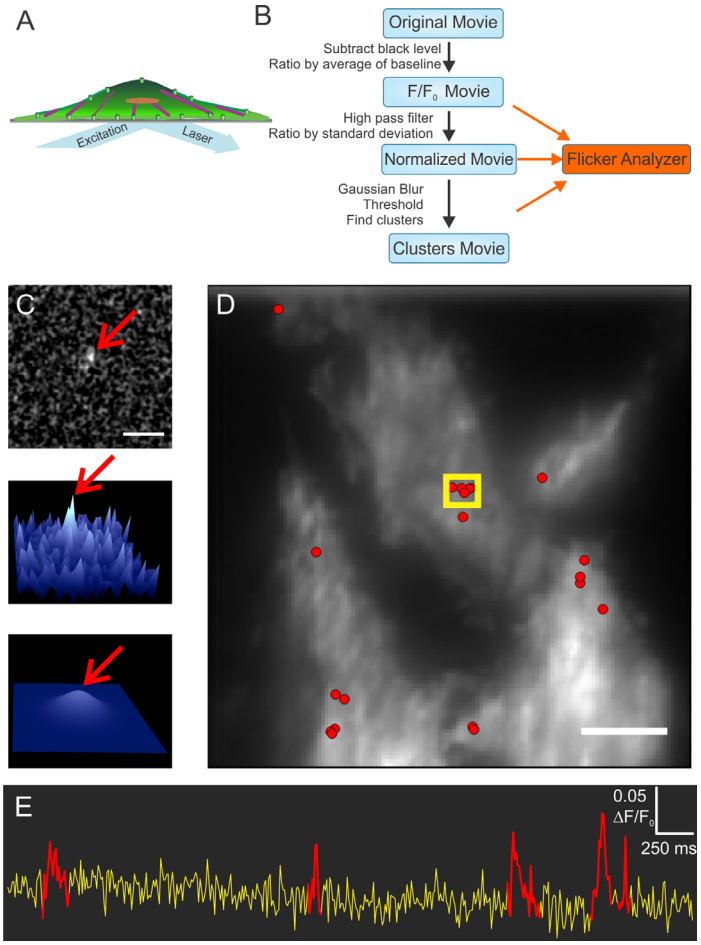

Figure 2. Automated detection and super-resolution localization of Piezo1 flickers. A. Piezo1 flickers are acquired by Ca^{2+} imaging with Total Internal Reflection Fluorescence Microscopy (TIRFM). **B.** Flowchart of the algorithm. The original movie is processed to subtract camera black level and then divided by the average of the first ~100 frames to produce a F/F_0 ratio movie. The ratioed movie is spatially and temporally filtered to increase the signal-to-noise ratio. A clustering algorithm groups supra-threshold pixels into flicker events. **C.** For every event detected, a 2D Gaussian fit to the fluorescence intensity identifies with sub-pixel accuracy the centroid of the fluorescence, and therefore of the ion channel(s) producing the Ca^{2+} signal. Representative images of a 200 µm x 200 µm region showing a processed, filtered Piezo1 flicker event (top, red arrow), a 3D representation of the event (middle) and the Gaussian fit to the event (bottom). Arrow in bottom panel marks the peak of the Gaussian profile that identifies with sub-pixel accuracy the location of the centroid of the Ca^{2+} flicker. **D.** Flicker localizations (red dots) overlaid on an image of an hNSPC to map sites of Piezo1 activity. E. Flicker activity from the region of interest marked in D plotted over time as fluorescence ratio changes ($\Delta F/F_0$). Identified flicker events are highlighted in red. Scale bars = 50 µm. See also Fig. S2.

Figure 2 shows an implementation of the algorithm applied to Piezo1 flickers recorded from hNSPCs (see also Movie M3 and Fig. S2). Piezo1 flickers are visualized by imaging Ca^{2+} influx through the channel using TIRFM (Fig. 2A). The raw movie is processed to produce a F/F_0 ratio movie (Fig. 2B) which is then spatially and temporally filtered to increase the signal-to-noise ratio of the signals of interest. The processed movie is passed through the clustering algorithm for event detection. Once events are detected, a 2-dimensional (2D) Gaussian curve is fit to every event in the movie to determine the localization of each flicker event with subpixel precision. Figure 1C shows the output of the algorithm for a single, representative flicker event after pre-processing steps (Fig. 2C, top and middle) and after the subpixel localization of the event by Gaussian fitting (Fig. 2C, bottom). The peak of this 2D Gaussian (red arrow, Fig. 2C bottom) identifies the center of the Ca^{2+} event with subpixel accuracy. Assuming the diffusion of

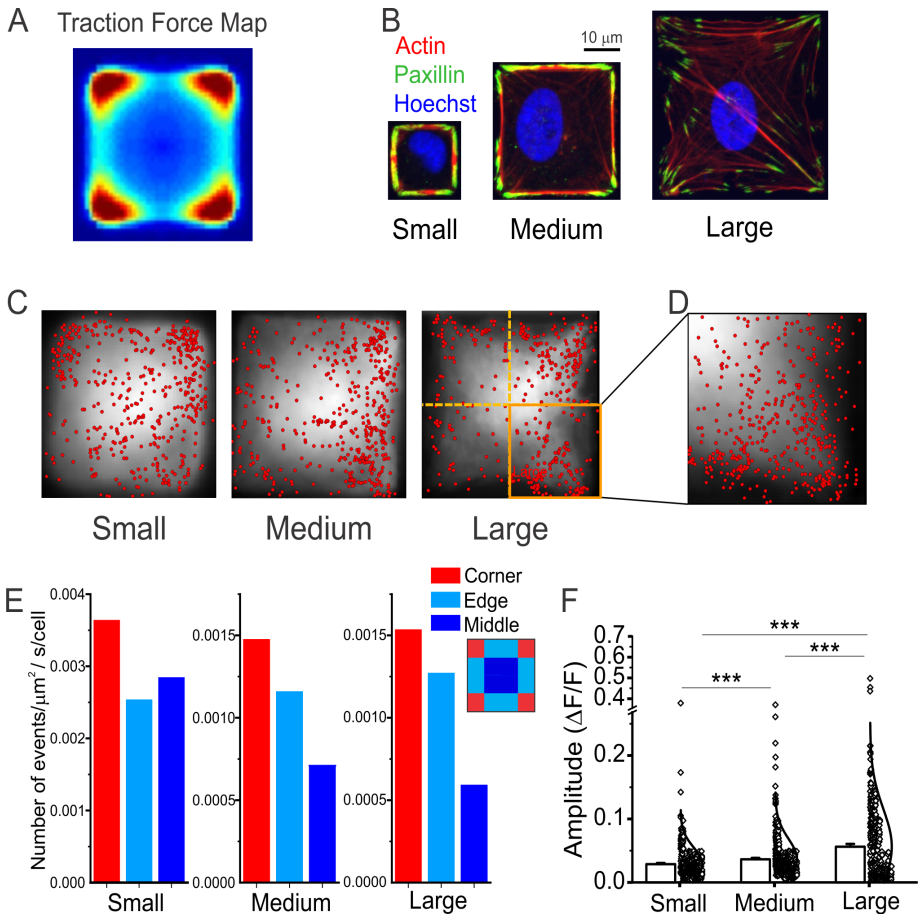

Figure 3. Piezo1 flickers are enriched in regions of cells predicted to have higher traction forces. A. Cells constrained to adopt a square shape on a patterned substrate generate the largest traction forces at the corners (red), lower levels of forces at the edges (cyan) and lowest traction forces in the middle of the cell. The image is reproduced from Holt et al. 2012 under CC BY-NC-SA 3.0 license. **B.** hNSPCs seeded on square fibronectin islands yield a single square cell per island. Images are representative confocal slices stained for the actin cytoskeleton (phalloidin, red), the focal adhesion zone protein, paxillin (anti-paxillin antibody, green), and the nucleus (Hoechst, blue). Note the larger number of actin stress fibers terminating in focal adhesions for cell adhering to larger islands. Island sizes used: Small, 300 μm²; Medium 1024 μm²; Large, 2025 μm². **C.** Localizations of Piezo1 flickers within cells seeded on Small, Medium, and Large islands. Each panel shows an image of a Cal520-loaded hNSPC, with an overlay of individual Piezo1 flicker localizations from multiple cells (red dots). The panels are shown scaled to the same size for ease of comparison. Total numbers of events represented in panels C, D, E are: Small, 453 events from 7 cells; Medium, 476 events from 7 cells; Large, 426 events from 4 cells. Data were acquired with an exposure time of 5ms (200 Hz frame rate). **D.** Flicker locations from all four quadrants of Large size mapped onto a single quadrant of a Cal520-loaded hNSPC. **E.** Frequencies of Piezo1 flickers in corner regions (red area in square inset), edge regions (light blue in inset), and middle region (dark blue, in inset) of cells grown on Small, Medium, and Large islands. Data are expressed as the number of events per μm² per second per cell. **F.** Bar and Data plot of flicker amplitudes for events from cells adhering to Small, Medium, and Large islands. Each dot represents an individual Piezo1 flicker event and bars denote the mean of all events for the specified cell size. Piezo1 flickers show greater amplitudes (ΔF/F) in cells seeded on large islands. *** denotes $p < 0.001$ by Kolmogorov-Smirnov test.

Ca^{2+} is radially symmetric, this gives the location of an individual ion channel, or the 'center of mass' of the group of ion channels, underlying the event. These flicker localizations are overlaid on an image of the cells (Fig. 2D) to produce a cellular map of active Piezo1 channels. The extracted signals can be analyzed to determine peak amplitude, temporal dynamics, and frequency of signals at a specific site (Fig. 2E). This technique made it possible for us to examine the spatial localization of Piezo1 activity in relation to cellular traction forces.

Piezo1 flickers are enriched at regions predicted to have high traction forces

To relate spatial maps of Piezo1 flicker activity to cellular traction forces, we mapped Piezo1 activity in cells generating known patterns of traction forces. We utilized the well-established effect of

cell geometry on traction forces: cell shape determines *where* forces are generated and cell size determines *how much* force is generated [42–45]. We controlled the shape and size of hNSPCs -- and therefore the spatial pattern and magnitude of their cellular traction forces -- using substrate micropatterning [35,36,45] and examined Piezo1 activity maps ian these micropatterned cells. To do so, glass coverslips were patterned with islands of fibronectin of pre-determined shapes and sizes. Upon seeding, cells bind to fibronectin via cellular integrins and take up the geometry of the island. We selected the shape of our substrate islands based on previous traction force measurements in micropatterned cells [42–44,46], which show that in cells constrained to a square shape, traction forces are highest at the vertices, moderately high at edges, and minimal in the center of the cell (Fig. 3A). Moreover, as the size of the square island is increased, the magnitude of traction force increases [43,45]. This robust dependence of traction forces on the shape and size of micropatterned square cells allowed us to ask whether the location and magnitude of Piezo1 flickers in square cells also shows a similar dependence on cell shape and size.

We seeded hNSPCs on glass substrates in square shapes of three different sizes (Small 17.3 μm x 17.3 μm= 300 μm^2, Medium 32 μm x 32 μm = 1024 μm^2, Large 45 μm x 45 μm = 2025 μm^2). We confirmed that micropatterned hNSPCs exhibited the shape and cytoskeletal organization expected of this geometry. For this, we visualized actin filaments in fixed micropatterned hNSPCs with fluorescently-labeled phalloidin, focal adhesions with an anti-Paxillin antibody, and cell nuclei with Hoechst dye (Fig. 3B). Cells on larger islands displayed greater numbers of, and longer, actin stress fibers, terminating in paxillin-rich focal adhesions that were concentrated in corner regions. Cells on Large islands displayed a network of actin stress fibers across the cell, while cells on Small islands showed actin accumulated primarily along the edges, as previously observed in other cell types for this specific set of square patterns [47].

Having determined that hNSPCs showed the expected cellular architecture when confined to square islands, we next imaged Piezo1 flickers in live cells adhering to Small, Medium, and Large islands and extracted their amplitudes and localizations (Fig. 3C-F). To determine the location of Piezo1 activity relative to the predicted traction force distribution, we determined the occurrence of flickers in three regions of the cell: Corner, Middle, and Edge regions normalized for area, as depicted in Fig. 3E. If flickers are randomly distributed, we would expect an equal occurrence of flickers in Corner, Middle, and Edge regions. However, we observed that for all three cell sizes, Corner regions showed more flickers per square micron per second (Fig. 3E). As cell spread area increased, the distribution of events shifted from the Middle region to Corner and Edge regions (Fig. 3C-E). Cells adhering to Small squares showed a higher frequency of flickers per square micron than those on Medium and Large squares, likely because cells with similar Piezo1 expression levels extend over a smaller surface area. Moreover, flicker amplitudes were greater in cells with a larger spread area (Fig. 3F), which are known to generate larger traction forces. Overall, our measurements show that Piezo1 flicker amplitudes scale with cell spread area, and that Piezo1 flickers are enriched in regions expected to have higher traction forces.

Piezo1 flickers localize to hotspots of traction forces

Our finding of enriched Piezo1 flickers in regions of micropatterned hNSPCs predicted to have higher traction forces motivated us to measure traction forces and Piezo1 flickers in the same cell. We used a Förster resonance energy transfer (FRET)-based molecular tension sensor (MTS) to measure cellular traction forces [48]. The MTS is comprised of an elastic peptide which separates a covalently-bound FRET pair (Fig. 4A). The N-terminus of the sensor is covalently attached to a functionalized glass coverslip to produce a carpet of sensors. The C-terminus of the MTS has a fibronectin fragment to which cells bind via integrins, such that cells seeded on to the sensor-coated glass coverslip adhere to the substrate via the MTS. Traction forces generated by the cell are communicated to the MTS via integrin-MTS attachments: these forces cause extension of the peptide spring, leading to a separation of the FRET pair and therefore a reduction in FRET efficiency. The FRET donor and acceptor channels are simultaneously imaged, yielding FRET index maps that are calculated by dividing the acceptor intensity over the sum of donor and acceptor intensities. A high FRET index indicates low traction force and a low FRET index indicates high traction force. The FRET index maps can be converted to FRET efficiency maps to allow

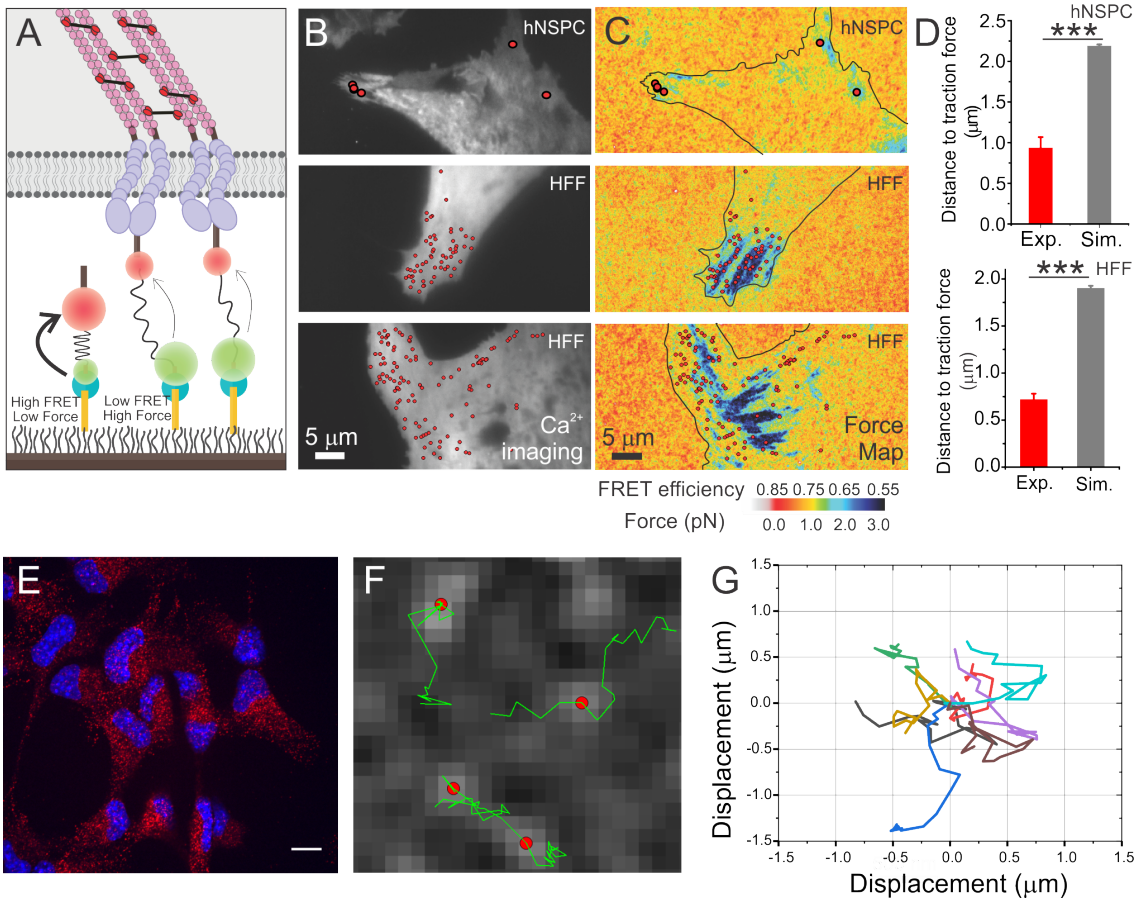

Figure 4. Piezo1 flickers localize to regions of high traction forces, while Piezo channels are motile and widely distributed. **A.** Schematic of the Molecular Tension Sensor (MTS) used for traction force imaging. The N-terminal region of the sensor (blue) is tethered to a PEG-functionalized glass coverslip. A fibronectin domain at the C-terminal end (brown) binds to the cell's integrins (purple), allowing cells to attach to the glass coverslip. An elastic spring domain bridges the two ends of the sensor and separates a FRET donor (green) and acceptor (red). Cell-generated traction forces pull the FRET pair apart, resulting in reduced FRET efficiency. The FRET index (the ratio of acceptor intensity over summed donor and acceptor intensities), serves as a measure of force; with a low FRET index indicating high force, and a high FRET index a low force. **B.** Ca^{2+} imaging of Piezo1 flickers. Panels show resting fluorescence of cells loaded with Ca^{2+} indicator Cal-520, with overlaid red dots marking the centroid locations of Ca^{2+} flickers. The top panel shows a representative image from an hNSPC, and the middle and bottom panels show images from two HFFs. **C.** Corresponding force maps from the same cells, overlaid with red dots marking the Ca^{2+} flicker locations. Blue denotes low FRET (high force) and red denotes high FRET (low force). The color bar in C represents FRET efficiency (top) and the average force per MTS per pixel in pN obtained from calibrated FRET-Force curves of the MTS as described in Methods. **D.** Red bars show mean distances from Piezo1 flicker localizations to the nearest traction force region for hNSPCs (top: 66 flickers from 18 cells) and HFFs (bottom: 515 flickers from 9 cells). Grey bars show corresponding mean distances derived from simulations of 1000 random intracellular locations for each cell. *** denotes $p < 0.001$ by Kolmogorov-Smirnov test. Error bars denote standard error of the mean. **E.** Single confocal slice image at the cell-coverslip surface of mNSPCs harvested from Piezo1-tdTomato reporter mice immunostained with an anti-RFP antibody (red) and Hoechst nuclear stain (blue). Note the widespread distribution of Piezo1-tdTomato channels across the cell membrane. Scale bar = 10 μm. **F.** Tracking of Piezo1-tdTomato channel puncta imaged at 10 fps in live mNSPCs reveals motility of channel puncta. The background image shows fluorescence of Piezo1-tdTomato puncta captured during a single imaging frame. Red dots mark the localizations of the puncta during that frame, and green lines depict the tracks of these puncta over several successive frames. Scale bar = 800 nm **G.** 'Flower plot' derived by overlaying the trajectories of 10 individual puncta over 1 second after normalizing their starting coordinates to the origin. See also Fig. S3, S4, and S5.

extraction of quantitative values for force based on the FRET-force response of the elastic peptide [39,49]; see Methods for details). Thus, imaging the donor and acceptor fluorophores allows the production of a quantitative, high-resolution traction force map of the cell. Compatibility of these sensors with TIR-FM-based Ca^{2+} imaging allowed us to measure and correlate cellular traction forces and Piezo1 activity in the same cell.

We seeded hNSPCs onto coverslips functionalized with the MTS, allowed the cells to attach and

spread for 1-2 hours, then loaded them with the Ca^{2+} indicator Cal-520 AM. We imaged traction forces followed by Piezo1 activity (Fig. 4B, C). Overlaying maps of Piezo1 flickers and force demonstrated that Piezo1 flickers occurred in regions of the cell that displayed high traction forces (Fig. 4C). To quantify the spatial relationship between traction forces and Piezo1 flickers, we calculated the distance of Piezo1 flickers to the nearest force-producing region (Fig. 4D). To determine whether the localization of Piezo1 flickers was different from chance, we simulated 1000 randomly localized Piezo1 flicker sites in each cell and compared the distance of experimental and randomly simulated Piezo1 flicker localizations to the nearest high-force region.

In hNSPCs experimental flickers were 0.94 μm away from high-force regions, whereas simulated flicker localizations were situated 2.2 μm away (Fig. 4D, top; $p < 0.001$ by Kolmogorov-Smirnov test). We also imaged force maps and Ca^{2+} flickers in human foreskin fibroblasts (HFFs), a popular cell type for studying traction forces because they display large adhesions which generate high traction forces [38,48,49]. On average, flicker localizations were located 0.72 μm from force-producing adhesions, whereas simulated flicker localizations were located at a distance of 1.9 μm from force-producing regions (Fig. 4D, bottom; $p < 0.001$ by Kolmogorov-Smirnov test). Together, our findings indicate that Piezo1 flicker location is spatially correlated with traction forces.

Piezo1 channels diffuse over the surface of the cell

The traction force produced by Myosin II is communicated through actin filaments to focal adhesions that attach to the substrate [50,51]. Our observation that Piezo1 flickers arise predominantly in the vicinity of force-producing focal adhesions suggested two possibilities: (i) Piezo1 channels are localized to focal adhesions where traction forces are transmitted to the substrate, or (ii) Piezo1 channels are present all over the cell surface, but are only activated by traction forces near force-producing adhesions. To distinguish between these possibilities we visualized the localization of Piezo1 proteins. The dearth of sensitive and specific antibodies against endogenous Piezo1 precluded immunolocalization of the native channel to answer this question. Instead, we used a knock-in reporter mouse wherein a tdTomato fluorescent protein is tagged to the C-terminus of the endogenous Piezo1 channel [5]. The expression of the Piezo1-tdTomato fusion protein is driven by the native Piezo1 promoter and regulatory elements; thus expression levels and patterns of the tagged channel are expected to be the same as that of endogenous channels. We immunostained endogenous Piezo1-tdTomato channels in mNSPCs with an anti-RFP antibody and observed channels distributed all over the cell surface rather than being localized to focal adhesions (Fig. 4E, S3).

Imaging of the tdTomato moiety in live mNSPCs at the cell-substrate interface by TIRF microscopy revealed that individual Piezo1 puncta are mobile in the plasma membrane (Fig. 4F-G, Movie M4). with an apparent two-dimensional diffusion coefficient of = $0.067 \mu m^2/s$ (Fig. S4). Using lattice light-sheet imaging, we further observed mobility of Piezo1 channels at the top, attachment-free, surface of the cell and at cell-cell interfaces (Fig. S5, Movies M5 and M6).

Taken together, the widespread distribution of Piezo1 channels on the cell surface and their mobility suggest that channels in the vicinity of focal adhesions are activated by local mechanical stresses produced by traction force generation, whereas the channels farther away remain largely silent.

Force generation by MLCK-mediated Myosin II phosphorylation activates Piezo1

Nonmuscle Myosin II hydrolyzes ATP to convert chemical energy into mechanical force, which is communicated through actin filaments and focal adhesions to the extracellular matrix (Fig. 5A). We previously showed that inhibition of Myosin II by blebbistatin inhibited Piezo1 flickers [7]. Myosin II activity is regulated by the Myosin II regulatory light chain subunit, whose phosphorylation converts Myosin II from an inactive form to an active form capable of filament assembly and force generation (Fig. 5A). We asked how the phosphorylation state of Myosin II might impact Piezo1 activity. Myosin II is phosphorylated by two kinases - Rho-associated protein kinase (ROCK) and Myosin Light Chain Kinase (MLCK). The two kinases control distinct spatial pools of Myosin II: ROCK phosphorylates Myosin II in the center of the cells while MLCK phosphorylates Myosin II in the periphery [52–54]. The ROCK inhib-

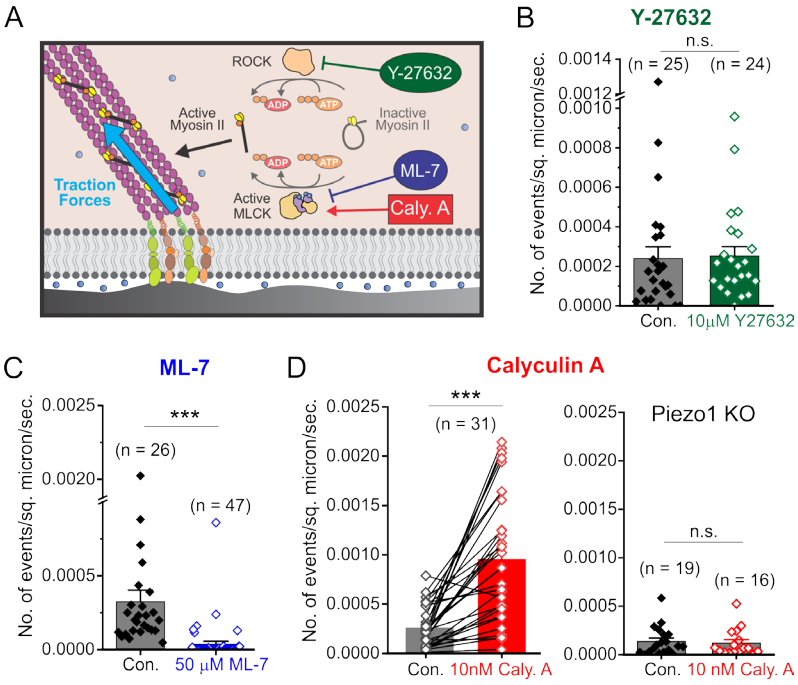

Figure 5. Piezo1 flickers are generated by the action of Myosin II motors. A. Schematic of traction force generation by Myosin II motors. The enzyme Myosin Light Chain Kinase (MLCK, beige and purple) phosphorylates Myosin II (yellow and black) to generate the activated form that binds actin filaments (purple) and produces traction forces (blue arrow). The drug ML-7 inhibits MLCK activity and the drug Calyculin A potentiates MLCK activity, to alter traction force generation by Myosin II. **B.** Treatment of HFFs by 10 nM Calyculin A increases the frequency of Piezo1 flickers. Left, Paired measurements of flicker frequency in the same fields of view in Control imaging solution and 1-5 minutes after replacement of imaging solution containing 10 nM Calyculin A. Right, 10 nM Calyculin A does not increase Ca^{2+} flickers in Piezo1-Knockout HFFs. Data are from three experiments; n.s. denotes "not statistically significant" by Kolmogorov-Smirnov test. In all graphs, bar height denotes the mean of the data points, error bars denote standard error of the mean, and the number of videos analyzed from 3 different experiments is specified for each condition. **C.** Treatment of HFFs with 10 μM of the ROCK inhibitor Y-27632 inhibits Piezo1 flickers. **D.** Treatment of HFFs with 50 μM ML-7 inhibits Piezo1 flickers. Bar and data plot of Piezo1 flicker frequency from WT HFFs in Control imaging solution and in the presence of 50 μM ML-7. In B-D bars denote mean ± sem and each point represents mean flicker frequency in an individual video. n values denote number of videos from three different experiments. Data are from three experiments. *** denotes $p < 0.001$ by Kolmogorov-Smirnov test. See also Fig. S6.

itor Y-27632 had no effect on Piezo1 flicker frequency (Fig. 5C). On the other hand, the MLCK inhibitor ML-7, which we previously showed to rapidly reduce traction force generation in HFFs [49], effectively inhibited Piezo1 flickers (Fig. 5D). The regulation of Piezo1 flickers by MLCK (which has been shown to phosphorylate Myosin II at the periphery of the cell) but not by ROCK (which activates Myosin II in the center of the cell) is consistent with the observation that Piezo1 flickers are more often observed in the periphery of cells (for example, see Piezo1 activity maps in Figs. 3 and 4).

Previous work establishes that treatment of cells with Calyculin A, an inhibitor of myosin light chain phosphatase, increases myosin-dependent force generation [55–57]. We found that Ca^{2+} flickers in the same set of HFFs before and after treatment with 10 nM Calyculin A showed on average 5-fold increase in Ca^{2+} flickers within minutes (Fig. 5B, left). Calyculin A failed to increase flicker activity in the absence of external Ca^{2+}, indicating that Ca^{2+} influx across the plasma membrane is required (Fig. S6). Piezo1 KO HFFs did not show increased flicker activity in response to Calyculin A (Fig. 5B, right), indicating that the observed increase in frequency of Ca^{2+} flickers is mediated by Piezo1. Overall, these results demonstrate that increased phosphorylation of Myosin II increases Piezo1 flickers. In summary, we link Piezo1 flickers to Nonmuscle Myosin II-generated mechanical forces and uncover an upstream signaling mechanism that regulates its activity.

DISCUSSION

Technical advances in Piezo1 activity measurements

Emerging evidence for a functional interplay of Piezo1 and the cellular cytoskeleton [1] emphasizes the need for studying Piezo1 activity in native cellular conditions and in conjunction with cytoskeletal dynamics. Towards this goal, we improved our TIRFM-based Piezo1 flicker assay [7] to provide a measure of Piezo1 activity at millisecond temporal and sub-micron spatial resolution. The greater signal-to-noise ratio afforded by TIRFM allowed detection of small signals arising from the activity of endogenously-expressed channels at the cell-substrate interface. We developed a custom-written, open-source

analysis algorithm that utilizes principles from localization microscopy for the automated detection, localization, and measurement of Ca^{2+} flickers.

Our approach complements electrophysiological assays of Piezo1 activity. It does not disrupt the cellular cytoskeleton or dialyze the cell, provides a measurement of channel dynamics under native cellular conditions, and allows spatial monitoring of Piezo1 activity that is not feasible with patch clamp electrophysiology. Finally, it permits an examination of Piezo1 activity in response to cell-generated forces, which are orders of magnitude lower than mechanical stimuli applied in patch clamp assays. Together, we provide a powerful experimental and analytical framework for examining the interplay between Piezo1 and the cytoskeleton.

Spatial regulation of Piezo1 activity by cellular traction forces

We combined our Piezo1 Ca^{2+} flicker assay with approaches to manipulate and measure intrinsic cellular traction forces. First, we used micropatterned square substrates to constrain the shape and size of cells such that they generate a known pattern of traction forces [35,36,45]. Piezo1 flickers were enhanced in corners and edges of these cells - regions predicted to have high traction forces (Fig. 3). Second, we used a FRET-based molecular tension sensor (MTS) [38,48] to quantitatively measure cellular traction forces and correlate cellular traction forces and Piezo1 activity in the same cell. These measurements would be difficult using conventional traction force microscopy (TFM), which tracks the displacement of fluorescent beads in a soft gel substrate, due to the technical challenges inherent in imaging Ca^{2+} flickers on soft substrates, as well as the limited spatial resolution of commonly implemented versions of TFM. We observed a clear spatial correlation between Piezo1 flickers and high traction forces, consistent with local cellular traction forces activating the channel.

Building on our previous finding that direct Nonmuscle Myosin II inhibition reversibly inhibits Piezo1 flickers [7], we now provide an upstream signaling mechanism responsible for activation of Piezo1 by Myosin II generated forces. We find that phosphorylation of Myosin II by MLCK is necessary for generating Piezo1 flickers. Interestingly, the Myosin II kinase ROCK does not seem to be involved in generating Piezo1 flickers. Given that MLCK is itself regulated by Ca^{2+}, it is interesting to speculate that MLCK, nonmuscle myosin II, and Piezo1 might constitute a feedforward loop whose activity could, hypothetically, concentrate myosin contractility in regions of the cytoskeleton proximal to load-bearing attachments to the ECM. Further experiments, beyond the scope of this study, will be required to test this possibility.

Piezo1 as a transducer of extracellular matrix mechanics

Extracellular matrix mechanics direct stem cell differentiation [58], cancer pathology [59], and cell migration [60]. The molecular mechanisms by which mechanical properties of the matrix are transduced into the biochemical signals that regulate intracellular processes are not fully understood. The prevailing view is that cells probe the elasticity of the matrix using actively-generated traction forces, much as a person would test the elasticity of an object by pulling on it [50]. When presented with stiffer substrates, cells respond by generating larger traction forces. Traction forces in turn determine a variety of downstream signaling processes through mechanisms that are not yet fully understood. We provide direct experimental evidence that cytoskeletal forces generated by the cell itself can activate the Piezo1 channel, which can in turn regulate cytosolic Ca^{2+} and downstream, intracellular signaling. In support of this model, stiffer substrates elicit greater Piezo1 activity than soft substrates [7], and Piezo1 is implicated in stiffness-driven axonal guidance in embryonic development [61].

Piezo1 channels are mobile

We find that Piezo1 channels are mobile in the cell membrane, with an apparent ensemble diffusion coefficient of 0.067 $\mu m^2/s$. This value is within the wide range of diffusion coefficients of 0.01 - 0.3 $\mu m^2/s$ measured for membrane proteins [62–65]. Whereas Piezo1 channels appear to diffuse readily in the plasma membrane, the restriction of flicker activity to regions of the cell that exhibit traction forces (Fig. 4) raises the possibility that active channels may be transiently anchored. A full analysis of Piezo1

subcellular localization and dynamics is beyond the scope of this study, but is likely to provide key insights into Piezo1-mediated mechanotransduction and the interaction of the channel with its cellular environment.

How do traction forces activate Piezo1?

Several studies have proposed that Piezo1 is gated by membrane tension [27,28,33,66], and three recent cryo-EM structures of Piezo1 [66–68] support this gating mechanism. Our working model for the activation of Piezo1 flickers by traction forces is that these forces produce a local increase in membrane tension which activates Piezo1 channels in the vicinity of force-producing adhesions (Fig. 6). In support of this idea, Piezo1 flickers are sometimes located proximal to, but not directly overlying the traction force hotspots (Fig. 4C, bottom).

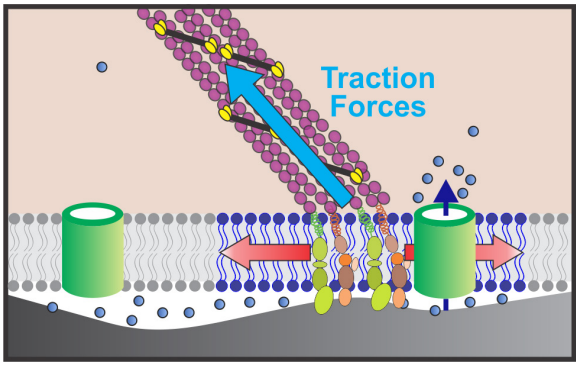

Figure 6. Working model of Piezo1 activation by traction forces. Traction forces (blue arrow) generated by Myosin II motors (yellow and black) along actin filaments (purple) tethered to integrin-based focal adhesion zones (green and brown) generate local increases in membrane tension (depicted by blue region of lipid bilayer and red arrows) that elicit Ca^{2+} flickers from nearby Piezo1 channels (green cylinder in right part of figure). Blue dots represent Ca^{2+} ions and dark blue arrow represents Ca^{2+} influx through Piezo1. Piezo1 channels far from force-producing adhesions are not activated (green cylinder in left of figure).

Whether membrane tension is a global or a local cellular parameter has been a subject of ongoing debate [69]. A recent study demonstrates that in intact cells -- unlike in membrane blebs -- perturbation to membrane tension can be a local event that does not necessarily propagate far [70]. Our study favors the model that local membrane tension induced by cytoskeletal forces activates Piezo1 (Fig. 6). However, we cannot presently exclude alternative possibilities including transient physical interactions between Piezo1 and focal adhesion proteins, and changes in membrane organization (e.g. in invaginations or folding) that may occur near traction force regions.

An open question is whether Piezo1 flickers represent the activity of single channels or a cluster of channels, and correspondingly, whether the motile Piezo1-tdTomato puncta represent individual channels or clusters of channels that move as a unit, as has been described for IP_3 receptors [71]. We observed a larger amplitude of Piezo1 flickers in larger cells, which have higher traction forces (Fig. 3). If flickers represent single-channel activations, then we would expect to observe changes in flicker frequency but not in amplitude. Thus, it is plausible that flickers represent the activity of clusters of channels, with higher forces activating a larger fraction of channels in the cluster. Consistent with this idea, Bae et al. [21] observed in cell-attached patch clamp experiments that groups of Piezo1 channels sometimes showed a collective change in dynamics, including a collective loss of inactivation or an abrupt change in activation kinetics. Alternatively, the measured amplitude differences could arise from bursts of unresolved individual openings.

An emerging picture of Piezo1 mechanotransduction

Piezo1 responds on the millisecond timescale to diverse external mechanical cues such as cell indentation [2], shear flow [4], membrane stretching [2,33], substrate displacement [30], and osmotic stress [28]. Some of these mechanical stimuli impinge upon a small region of the cell, whereas others affect the cell in its entirety. How then may Piezo1 channels quickly respond to mechanical cues that may strike anywhere and at any time in the cell while also transducing cell-generated traction forces that occur specifically at focal adhesion zones? We propose that -- like policemen patrolling a city -- mobility allows a smaller number of Piezo1 channels to explore a larger number of mechanical microdomains, and thereby respond to a diversity of mechanical cues efficiently. Whereas the electrical signal generated from Piezo1 ion flux would globally depolarize the cell, the restricted nature of Ca^{2+} diffusion in the cytosol tightly constrains the 'chemical' signal to the vicinity of the channel. Thus, spatial localization of Piezo1 activity could serve to spatially localize biochemical signaling downstream of Piezo1, and may be a key component rendering specificity to its diverse physiologic roles in different cell types.

ACKNOWLEDGEMENTS

We thank Truc Tran, Nhu Nguyen, Huixun Du, Klara Zakery Juhi Gopal, Brian Nguyen, and Chang Zhao for technical assistance; Vivian Leung for help with manuscript preparation; Dr. Douglas Tobias and members of Pathak lab for discussions; and Dr. Ardem Patapoutian for the gift of Piezo1-td-Tomato mice. This work was supported by NIH grants DP2 AT010376R21 and R01 NS109810 to M. M. P., NS085628 to F. T., R37 GM048071 to I.P, F31 GM119330 to K.E., R01 GM112998 and an HHMI Faculty Scholar Award to A.R.D., CIRM RB5-07254 to L.A.F. and T32 NS082174 to J.A.

DECLARATION OF INTERESTS

The authors declare no competing interests.

REFERENCES

1. Nourse, J.L., and Pathak, M.M. (2017). How cells channel their stress: Interplay between Piezo1 and the cytoskeleton. Semin. Cell Dev. Biol. 71, 3–12.
2. Coste, B., Mathur, J., Schmidt, M., Earley, T.J., Ranade, S., Petrus, M.J., Dubin, A.E., and Patapoutian, A. (2010). Piezo1 and Piezo2 are essential components of distinct mechanically activated cation channels. Science 330, 55–60.
3. Coste, B., Xiao, B., Santos, J.S., Syeda, R., Grandl, J., Spencer, K.S., Kim, S.E., Schmidt, M., Mathur, J., Dubin, A.E., et al. (2012). Piezo proteins are pore-forming subunits of mechanically activated channels. Nature 483, 176–181.
4. Li, J., Hou, B., Tumova, S., Muraki, K., Bruns, A., Ludlow, M.J., Sedo, A., Hyman, A.J., McKeown, L., Young, R.S., et al. (2014). Piezo1 integration of vascular architecture with physiological force. Nature 515, 279–282.
5. Ranade, S.S., Qiu, Z., Woo, S.-H., Hur, S.S., Murthy, S.E., Cahalan, S.M., Xu, J., Mathur, J., Bandell, M., Coste, B., et al. (2014). Piezo1, a mechanically activated ion channel, is required for vascular development in mice. Proc. Natl. Acad. Sci. U. S. A. 111, 10347–10352.
6. Sugimoto, A., Miyazaki, A., Kawarabayashi, K., Shono, M., Akazawa, Y., Hasegawa, T., Ueda-Yamaguchi, K., Kitamura, T., Yoshizaki, K., Fukumoto, S., et al. (2017). Piezo type mechanosensitive ion channel component 1 functions as a regulator of the cell fate determination of mesenchymal stem cells. Sci. Rep. 7, 17696.
7. Pathak, M.M., Nourse, J.L., Tran, T., Hwe, J., Arulmoli, J., Le, D.T.T., Bernardis, E., Flanagan, L.A., and Tombola, F. (2014). Stretch-activated ion channel Piezo1 directs lineage choice in human neural stem cells. Proc. Natl. Acad. Sci. U. S. A. 111, 16148–16153.
8. Gudipaty, S.A., Lindblom, J., Loftus, P.D., Redd, M.J., Edes, K., Davey, C.F., Krishnegowda, V., and Rosenblatt, J. (2017). Mechanical stretch triggers rapid epithelial cell division through Piezo1. Nature 543, 118–121.
9. Miyamoto, T., Mochizuki, T., Nakagomi, H., Kira, S., Watanabe, M., Takayama, Y., Suzuki, Y., Koizumi, S., Takeda, M., and Tominaga, M. (2014). Functional role for Piezo1 in stretch-evoked Ca2+ influx and ATP release in urothelial cell cultures. J. Biol. Chem. 289, 16565–16575.
10. Cahalan, S.M., Lukacs, V., Ranade, S.S., Chien, S., Bandell, M., and Patapoutian, A. (2015). Piezo1 links mechanical forces to red blood cell volume. Elife 4. Available at: http://dx.doi.org/10.7554/eLife.07370.
11. Hung, W.-C., Yang, J.R., Yankaskas, C.L., Wong, B.S., Wu, P.-H., Pardo-Pastor, C., Serra, S.A., Chiang, M.-J., Gu, Z., Wirtz, D., et al. (2016). Confinement Sensing and Signal Optimization via Piezo1/PKA and Myosin II Pathways. Cell Rep. 15, 1430–1441.
12. Li, C., Rezania, S., Kammerer, S., Sokolowski, A., Devaney, T., Gorischek, A., Jahn, S., Hackl, H.,

Groschner, K., Windpassinger, C., et al. (2015). Piezo1 forms mechanosensitive ion channels in the human MCF-7 breast cancer cell line. Sci. Rep. 5, 8364.

13. McHugh, B.J., Murdoch, A., Haslett, C., and Sethi, T. (2012). Loss of the integrin-activating transmembrane protein Fam38A (Piezo1) promotes a switch to a reduced integrin-dependent mode of cell migration. PLoS One 7, e40346.
14. Retailleau, K., Duprat, F., Arhatte, M., Ranade, S.S., Peyronnet, R., Martins, J.R., Jodar, M., Moro, C., Offermanns, S., Feng, Y., et al. (2015). Piezo1 in Smooth Muscle Cells Is Involved in Hypertension-Dependent Arterial Remodeling. Cell Rep. 13, 1161–1171.
15. Rocio Servin-Vences, M., Moroni, M., Lewin, G.R., and Poole, K. (2017). Direct measurement of TRPV4 and PIEZO1 activity reveals multiple mechanotransduction pathways in chondrocytes. Elife 6. Available at: http://dx.doi.org/10.7554/eLife.21074.
16. Lee, W., Leddy, H.A., Chen, Y., Lee, S.H., Zelenski, N.A., McNulty, A.L., Wu, J., Beicker, K.N., Coles, J., Zauscher, S., et al. (2014). Synergy between Piezo1 and Piezo2 channels confers high-strain mechanosensitivity to articular cartilage. Proc. Natl. Acad. Sci. U. S. A. 111, E5114–22.
17. Wang, S., Chennupati, R., Kaur, H., Iring, A., Wettschureck, N., and Offermanns, S. (2016). Endothelial cation channel PIEZO1 controls blood pressure by mediating flow-induced ATP release. J. Clin. Invest. 126, 4527–4536.
18. Rode, B., Shi, J., Endesh, N., Drinkhill, M.J., Webster, P.J., Lotteau, S.J., Bailey, M.A., Yuldasheva, N.Y., Ludlow, M.J., Cubbon, R.M., et al. (2017). Piezo1 channels sense whole body physical activity to reset cardiovascular homeostasis and enhance performance. Nat. Commun. 8, 350.
19. Albuisson, J., Murthy, S.E., Bandell, M., Coste, B., Louis-Dit-Picard, H., Mathur, J., Fénéant-Thibault, M., Tertian, G., de Jaureguiberry, J.-P., Syfuss, P.-Y., et al. (2013). Dehydrated hereditary stomatocytosis linked to gain-of-function mutations in mechanically activated PIEZO1 ion channels. Nat. Commun. 4, 1884.
20. Andolfo, I., Alper, S.L., De Franceschi, L., Auriemma, C., Russo, R., De Falco, L., Vallefuoco, F., Esposito, M.R., Vandorpe, D.H., Shmukler, B.E., et al. (2013). Multiple clinical forms of dehydrated hereditary stomatocytosis arise from mutations in PIEZO1. Blood 121, 3925–35, S1–12.
21. Bae, C., Gnanasambandam, R., Nicolai, C., Sachs, F., and Gottlieb, P.A. (2013). Xerocytosis is caused by mutations that alter the kinetics of the mechanosensitive channel PIEZO1. Proc. Natl. Acad. Sci. U. S. A. 110, E1162–8.
22. Zarychanski, R., Schulz, V.P., Houston, B.L., Maksimova, Y., Houston, D.S., Smith, B., Rinehart, J., and Gallagher, P.G. (2012). Mutations in the mechanotransduction protein PIEZO1 are associated with hereditary xerocytosis. Blood 120, 1908–1915.
23. Spier, I., Kerick, M., Drichel, D., Horpaopan, S., Altmüller, J., Laner, A., Holzapfel, S., Peters, S., Adam, R., Zhao, B., et al. (2016). Exome sequencing identifies potential novel candidate genes in patients with unexplained colorectal adenomatous polyposis. Fam. Cancer 15, 281–288.
24. Fotiou, E., Martin-Almedina, S., Simpson, M.A., Lin, S., Gordon, K., Brice, G., Atton, G., Jeffery, I., Rees, D.C., Mignot, C., et al. (2015). Novel mutations in PIEZO1 cause an autosomal recessive generalized lymphatic dysplasia with non-immune hydrops fetalis. Nat. Commun. 6, 8085.
25. Lukacs, V., Mathur, J., Mao, R., Bayrak-Toydemir, P., Procter, M., Cahalan, S.M., Kim, H.J., Bandell, M., Longo, N., Day, R.W., et al. (2015). Impaired PIEZO1 function in patients with a novel autosomal recessive congenital lymphatic dysplasia. Nat. Commun. 6, 8329.
26. Ma, S., Cahalan, S., Lohia, R., LaMonte, G., Zeng, W., Murthy, S., Paytas, E., Grubaugh, N.D., Gamini, R., Berry, L., et al. (2017). Common Piezo1 allele in African populations causes xerocytosis and attenuates Plasmodium infection. bioRxiv, 159830. Available at: https://www.biorxiv.org/content/early/2017/07/06/159830.abstract [Accessed August 6, 2018].
27. Cox, C.D., Bae, C., Ziegler, L., Hartley, S., Nikolova-Krstevski, V., Rohde, P.R., Ng, C.-A., Sachs, F.,

Gottlieb, P.A., and Martinac, B. (2016). Removal of the mechanoprotective influence of the cytoskeleton reveals PIEZO1 is gated by bilayer tension. Nat. Commun. 7, 10366.

28. Syeda, R., Florendo, M.N., Cox, C.D., Kefauver, J.M., Santos, J.S., Martinac, B., and Patapoutian, A. (2016). Piezo1 Channels Are Inherently Mechanosensitive. Cell Rep. 17, 1739–1746.
29. Gottlieb, P.A., Bae, C., and Sachs, F. (2012). Gating the mechanical channel Piezo1: a comparison between whole-cell and patch recording. Channels 6, 282–289.
30. Poole, K., Herget, R., Lapatsina, L., Ngo, H.-D., and Lewin, G.R. (2014). Tuning Piezo ion channels to detect molecular-scale movements relevant for fine touch. Nat. Commun. 5, 3520.
31. Chen, C.S. (2008). Mechanotransduction - a field pulling together? J. Cell Sci. 121, 3285–3292.
32. Suchyna, T.M., Markin, V.S., and Sachs, F. (2009). Biophysics and structure of the patch and the gigaseal. Biophys. J. 97, 738–747.
33. Lewis, A.H., and Grandl, J. (2015). Mechanical sensitivity of Piezo1 ion channels can be tuned by cellular membrane tension. Elife 4. Available at: http://dx.doi.org/10.7554/eLife.12088.
34. Gaub, B.M., and Müller, D.J. (2017). Mechanical Stimulation of Piezo1 Receptors Depends on Extracellular Matrix Proteins and Directionality of Force. Nano Lett. 17, 2064–2072.
35. Singhvi, R., Kumar, A., Lopez, G.P., Stephanopoulos, G.N., Wang, D.I., Whitesides, G.M., and Ingber, D.E. (1994). Engineering cell shape and function. Science 264, 696–698.
36. Chen, C.S., Mrksich, M., Huang, S., Whitesides, G.M., and Ingber, D.E. (1997). Geometric control of cell life and death. Science 276, 1425–1428.
37. Stabley, D.R., Jurchenko, C., Marshall, S.S., and Salaita, K.S. (2011). Visualizing mechanical tension across membrane receptors with a fluorescent sensor. Nat. Methods 9, 64–67.
38. Morimatsu, M., Mekhdjian, A.H., Adhikari, A.S., and Dunn, A.R. (2013). Molecular tension sensors report forces generated by single integrin molecules in living cells. Nano Lett. 13, 3985–3989.
39. Grashoff, C., Hoffman, B.D., Brenner, M.D., Zhou, R., Parsons, M., Yang, M.T., McLean, M.A., Sligar, S.G., Chen, C.S., Ha, T., et al. (2010). Measuring mechanical tension across vinculin reveals regulation of focal adhesion dynamics. Nature 466, 263–266.
40. Ellefsen, K.L., Settle, B., Parker, I., and Smith, I.F. (2014). An algorithm for automated detection, localization and measurement of local calcium signals from camera-based imaging. Cell Calcium 56, 147–156.
41. Rodriguez, A., and Laio, A. (2014). Clustering by fast search and find of density peaks. Science 344, 1492–1496.
42. Parker, K.K., Brock, A.L., Brangwynne, C., Mannix, R.J., Wang, N., Ostuni, E., Geisse, N.A., Adams, J.C., Whitesides, G.M., and Ingber, D.E. (2002). Directional control of lamellipodia extension by constraining cell shape and orienting cell tractional forces. FASEB J. 16, 1195–1204.
43. Tan, J.L., Tien, J., Pirone, D.M., Gray, D.S., Bhadriraju, K., and Chen, C.S. (2003). Cells lying on a bed of microneedles: an approach to isolate mechanical force. Proc. Natl. Acad. Sci. U. S. A. 100, 1484–1489.
44. Wang, N., Ostuni, E., Whitesides, G.M., and Ingber, D.E. (2002). Micropatterning tractional forces in living cells. Cell Motil. Cytoskeleton 52, 97–106.
45. Théry, M. (2010). Micropatterning as a tool to decipher cell morphogenesis and functions. J. Cell Sci. 123, 4201–4213.
46. Holt, B.D., Shams, H., Horst, T.A., Basu, S., Rape, A.D., Wang, Y.-L., Rohde, G.K., Mofrad, M.R.K., Islam, M.F., and Dahl, K.N. (2012). Altered cell mechanics from the inside: dispersed single wall carbon nanotubes integrate with and restructure actin. J. Funct. Biomater. 3, 398–417.
47. Dupont, S., Morsut, L., Aragona, M., Enzo, E., Giulitti, S., Cordenonsi, M., Zanconato, F., Le Digabel, J., Forcato, M., Bicciato, S., et al. (2011). Role of YAP/TAZ in mechanotransduction. Nature 474,

179–183.

48. Chang, A.C., Mekhdjian, A.H., Morimatsu, M., Denisin, A.K., Pruitt, B.L., and Dunn, A.R. (2016). Single molecule force measurements in living cells reveal a minimally tensioned integrin state. ACS Nano 10, 10745–10752.
49. Morimatsu, M., Mekhdjian, A.H., Chang, A.C., Tan, S.J., and Dunn, A.R. (2015). Visualizing the interior architecture of focal adhesions with high-resolution traction maps. Nano Lett. 15, 2220–2228.
50. Discher, D.E., Janmey, P., and Wang, Y.-L. (2005). Tissue cells feel and respond to the stiffness of their substrate. Science 310, 1139–1143.
51. Geiger, B., Spatz, J.P., and Bershadsky, A.D. (2009). Environmental sensing through focal adhesions. Nat. Rev. Mol. Cell Biol. 10, 21–33.
52. Totsukawa, G., Yamakita, Y., Yamashiro, S., Hartshorne, D.J., Sasaki, Y., and Matsumura, F. (2000). Distinct roles of ROCK (Rho-kinase) and MLCK in spatial regulation of MLC phosphorylation for assembly of stress fibers and focal adhesions in 3T3 fibroblasts. J. Cell Biol. 150, 797–806.
53. Katoh, K., Kano, Y., Amano, M., Kaibuchi, K., and Fujiwara, K. (2001). Stress fiber organization regulated by MLCK and Rho-kinase in cultured human fibroblasts. Am. J. Physiol. Cell Physiol. 280, C1669–79.
54. Tanner, K., Boudreau, A., Bissell, M.J., and Kumar, S. (2010). Dissecting regional variations in stress fiber mechanics in living cells with laser nanosurgery. Biophys. J. 99, 2775–2783.
55. Lemmon, C.A., Chen, C.S., and Romer, L.H. (2009). Cell traction forces direct fibronectin matrix assembly. Biophys. J. 96, 729–738.
56. Raman, P.S., Paul, C.D., Stroka, K.M., and Konstantopoulos, K. (2013). Probing cell traction forces in confined microenvironments. Lab Chip 13, 4599–4607.
57. Jiang, J., Zhang, Z.-H., Yuan, X.-B., and Poo, M.-M. (2015). Spatiotemporal dynamics of traction forces show three contraction centers in migratory neurons. J. Cell Biol. 209, 759–774.
58. Smith, L.R., Cho, S., and Discher, D.E. (2018). Stem Cell Differentiation is Regulated by Extracellular Matrix Mechanics. Physiology 33, 16–25.
59. Rianna, C., Kumar, P., and Radmacher, M. (2018). The role of the microenvironment in the biophysics of cancer. Semin. Cell Dev. Biol. 73, 107–114.
60. van Helvert, S., Storm, C., and Friedl, P. (2018). Mechanoreciprocity in cell migration. Nat. Cell Biol. 20, 8–20.
61. Koser, D.E., Thompson, A.J., Foster, S.K., Dwivedy, A., Pillai, E.K., Sheridan, G.K., Svoboda, H., Viana, M., Costa, L. da F., Guck, J., et al. (2016). Mechanosensing is critical for axon growth in the developing brain. Nat. Neurosci. 19, 1592–1598.
62. Smith, I.F., Swaminathan, D., Dickinson, G.D., and Parker, I. (2014). Single-molecule tracking of inositol trisphosphate receptors reveals different motilities and distributions. Biophys. J. 107, 834–845.
63. Marlar, S., Arnspang, E.C., Pedersen, G.A., Koffman, J.S., and Nejsum, L.N. (2014). Measuring localization and diffusion coefficients of basolateral proteins in lateral versus basal membranes using functionalized substrates and kICS analysis. Biochim. Biophys. Acta 1838, 2404–2411.
64. Pantazaka, E., and Taylor, C.W. (2011). Differential distribution, clustering, and lateral diffusion of subtypes of the inositol 1,4,5-trisphosphate receptor. J. Biol. Chem. 286, 23378–23387.
65. Diffusion coefficient of plasma membrane prot - Generic - BNID 114189 Available at: http://bionumbers.hms.harvard.edu/bionumber.aspx?id=114189&ver=1 [Accessed April 1, 2018].
66. Guo, Y.R., and MacKinnon, R. (2017). Structure-based membrane dome mechanism for Piezo mechanosensitivity. Elife 6. Available at: http://dx.doi.org/10.7554/eLife.33660.
67. Zhao, Q., Zhou, H., Chi, S., Wang, Y., Wang, J., Geng, J., Wu, K., Liu, W., Zhang, T., Dong, M.-Q., et al. (2018). Structure and mechanogating mechanism of the Piezo1 channel. Nature 554, 487–492.

68. Saotome, K., Murthy, S.E., Kefauver, J.M., Whitwam, T., Patapoutian, A., and Ward, A.B. (2017). Structure of the mechanically activated ion channel Piezo1. Nature. Available at: http://dx.doi.org/10.1038/nature25453.

69. Diz-Muñoz, A., Fletcher, D.A., and Weiner, O.D. (2013). Use the force: membrane tension as an organizer of cell shape and motility. Trends Cell Biol. 23, 47–53.

70. Shi, Z., Graber, Z.T., Baumgart, T., Stone, H.A., and Cohen, A.E. (2018). Cell membranes resist flow. bioRxiv, 290643. Available at: https://www.biorxiv.org/content/early/2018/03/28/290643 [Accessed April 1, 2018].

71. Thillaiappan, N.B., Chavda, A.P., Tovey, S.C., Prole, D.L., and Taylor, C.W. (2017). Ca2+ signals initiate at immobile IP3 receptors adjacent to ER-plasma membrane junctions. Nat. Commun. 8, 1505.

Supplemental Figures

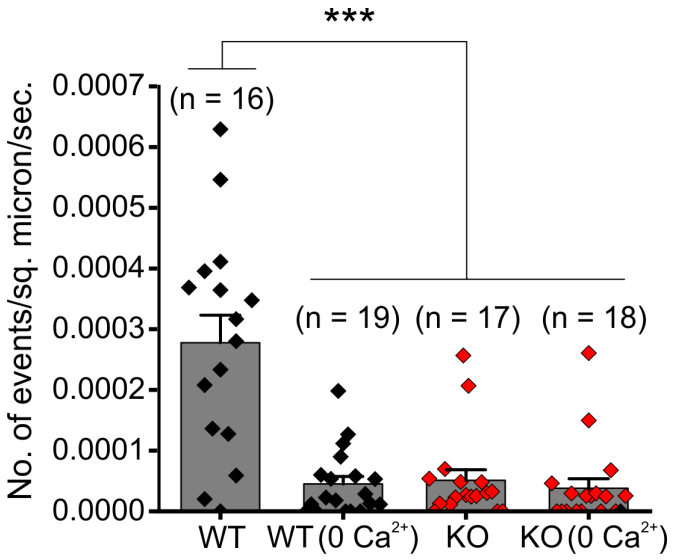

Figure S1. Residual Ca^{2+} flickers in Piezo1-knockout HFFs are mediated by intracellular Ca^{2+} release. Related to Fig. 1. Ca^{2+} flickers in WT HFF cells are reduced in Ca^{2+}-free extracellular solution (denoted as "0 Ca^{2+}"). Piezo1-knockout HFF cells in standard 3 mM extracellular Ca^{2+} exhibit Ca^{2+} flickers to a similar extent as WT (0 Ca^{2+}) cells, and these residual flickers are not eliminated in Ca^{2+}-free extracellular solution. Taken together, these observations suggest that residual Ca^{2+} flickers in Piezo1-knockout HFFs occur due to intracellular Ca^{2+} release. *** $p < 0.001$ by Kolmogorov-Smirnov test.

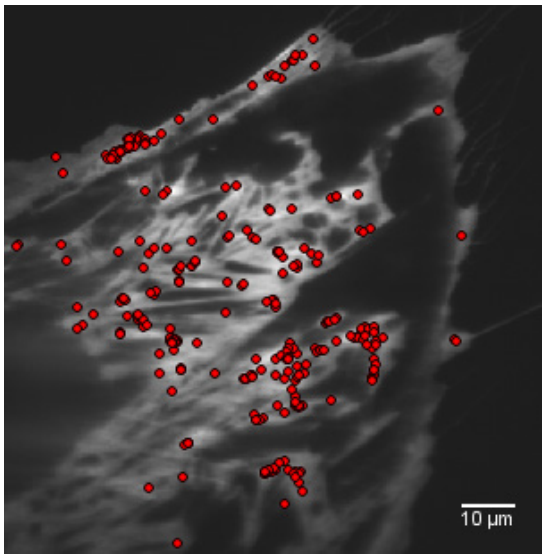

Figure S2. Piezo1 flicker localizations extracted from Movie S1. Related to Fig 2. Ca^{2+} flickers from HFF Movie M1 were analyzed as described in Fig. 2 and Methods.

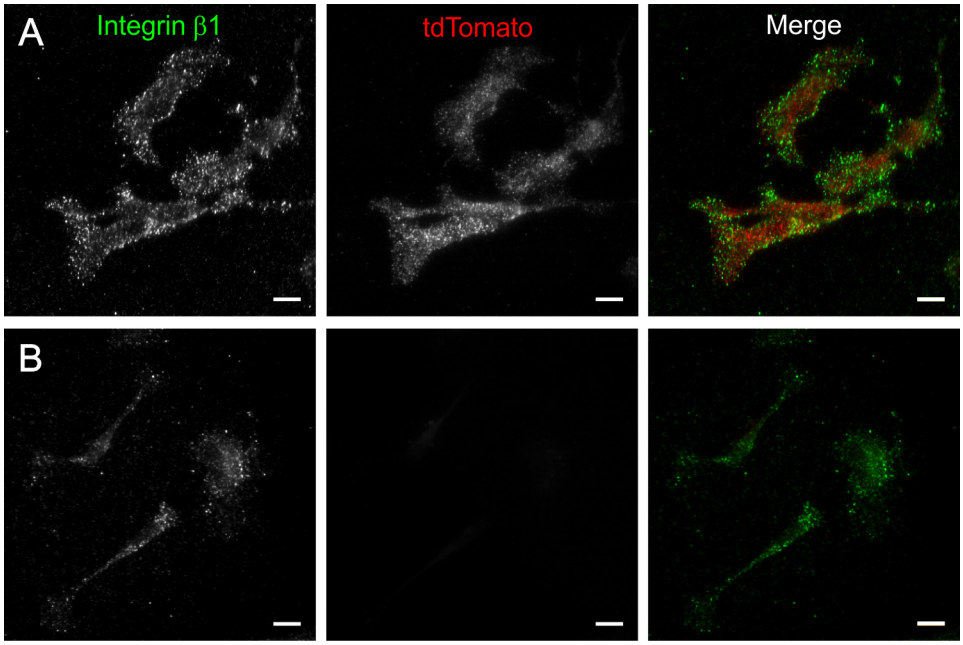

Figure S3. Piezo1 expression is not restricted to integrin-rich focal adhesions. Related to Fig 4. Representative TIR-FM images of mNSPCs immuno-labeled with antibody against Integrin b1 (green) and tdTomato (red): A, mNSPCs harvested from Piezo1-tdTomato reporter mice; B, mNSCPs harvested from wildtype mice. Scale bar = 10 µm

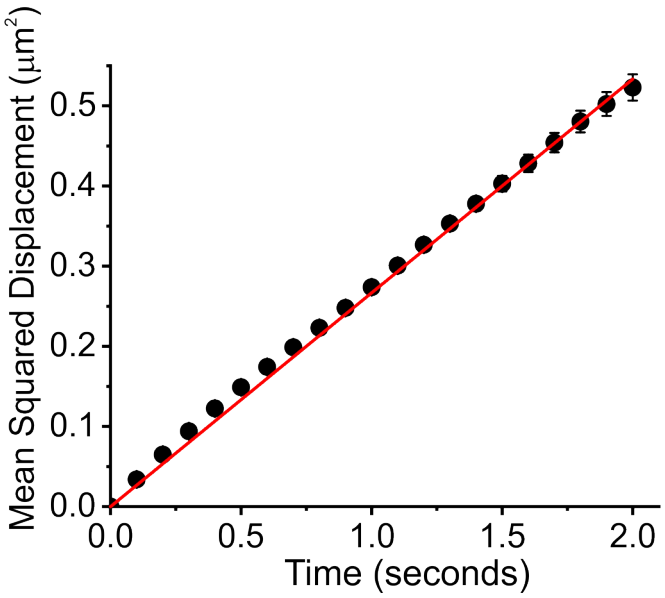

Figure S4. Diffusion coefficient of Piezo1 mobility. Related to Fig. 4. The slope of an ensemble Mean Squared Displacement (MSD) plot yielded an apparent two-dimensional diffusion coefficient of = 0.067μm²/s.

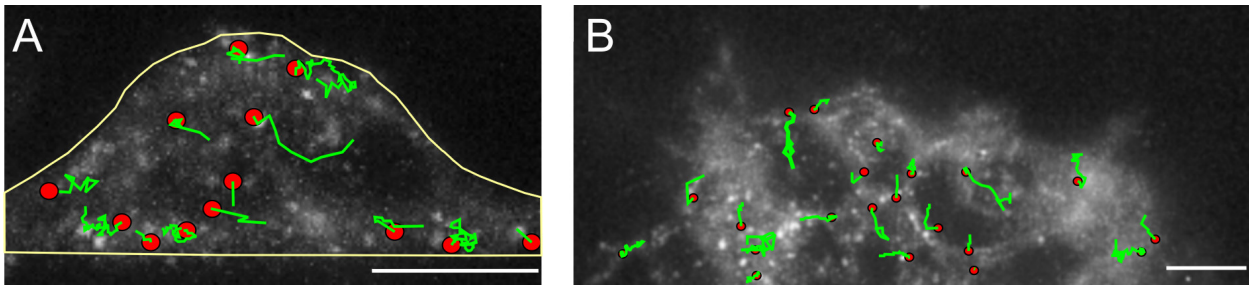

Figure S5. Lattice light-sheet imaging shows Piezo1 channels are motile on all surfaces of the cell. Related to Fig. 4. Imaging of Piezo1-tdTomato protein in mNSPCs by lattice light-sheet microscopy in a single cell (A) and in neurospheres (B). The background images show a maximum intensity projection of the entire movie. Red dots and green tracks mark trajectories of a subset of single puncta in contiguous frames. Yellow lines in A depict the outline of the cell imaged. Images were acquired every 50 ms. Scale bars = 10 μm.

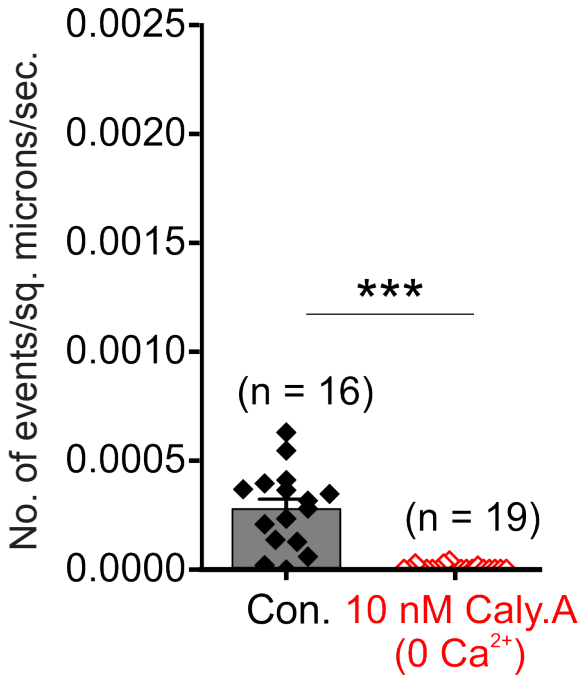

Figure S6. Increase in Ca^{2+} flickers with Calyculin A requires external Ca^{2+}. Related to Fig 5. Flicker frequency in Control imaging solution and 1-5 minutes after replacing the control bath solution with 10 nM Calyculin A in Ca^{2+}-free imaging solution (i.e. standard imaging solution containing 2 mM EGTA and no $CaCl_2$). Bars denote Mean ± sem and each point represents flicker frequency in an individual video. Data are from three experiments. *** denotes $p < 0.001$ by Kolmogorov-Smirnov test.

Movies

Movie M1. Piezo1 Ca^{2+} flickers are reduced in Piezo1-knockout HFFs. The movie shows an F/F_0 ratio movie of Ca^{2+} flickers from WT and Piezo1-KO HFFs.

Movie M2. Piezo1 Ca^{2+} flickers are reduced in Piezo1-knockout MEFs. The movie shows an F/F_0 ratio movie of Ca^{2+} flickers from WT and Piezo1-KO MEFs.

Movie M3. Piezo1 Ca^{2+} flickers imaged from HFFs. The movie shows the F/F_0 ratio movie from WT HFFs that was used for localization of Piezo1 flickers in Fig. S3.

Movie M4. Mobility of Piezo1-tdTomato puncta in mNSPCs imaged using TIRFM. Particles visible outside the yellow cell line are from neighboring cells.

Movie M5. Mobility of Piezo1-tdTomato puncta imaged by lattice light-sheet microscopy in a single mNSPC.

Movie M6. Mobility of Piezo1-tdTomato puncta in a mNSPC neurosphere imaged by lattice light-sheet microscopy.

Materials and Methods

Cell Culture

hNSPC Culture. Brain-derived fetal hNSPC cultures (SC27) were isolated from the cerebral cortex of a male fetus of 23-wk gestational age and were maintained as previously described (Pathak et al. 2014). Briefly, undifferentiated cells were grown as adherent cultures on fibronectin (Fisher Scientific)-coated flasks in basal medium containing DMEM/F12 (GIBCO), 20% BIT-9500 (Stem Cell Technologies), and 1% antibiotic/antimycotic (Invitrogen) supplemented with the following growth factors: 40 ng/mL EGF (BD Biosciences), 40 ng/mL FGF (BD Biosciences), and 40 ng/mL PDGF (Peprotech). hNSPCs were passaged approximately every 5-7 days using Cell Dissociation Buffer (Invitrogen) and split 1:2. Cells were used at passages P10–22. Informed written consent was obtained for all human subjects.

mNSPC Culture. NSPCs from cerebral cortices of E12.5 wildtype mice or from mice expressing a C-terminal fusion of Piezo1 with tdTomato (Piezo-tdTomato) (Ranade et al. 2014) were cultured as neurospheres as described previously(Nourse et al. 2014). Piezo1-tdTomato reporter mice were a gift from A. Patapoutian. mNSPC growth medium consisted of: High glucose Dulbecco's modified Eagle's medium (all reagents from Life Technologies unless otherwise noted), 1x B27, 1x N2, 1 mM sodium pyruvate, 2 mM glutamine, 1 mM N-acetylcysteine (Sigma Aldrich), 20 ng/ml epidermal growth factor (EGF) (BD Biosciences), 10 ng/ml fibroblast growth factor (FGF) (BD Biosciences), and 2 µg/ml heparin (Sigma Aldrich). Cells were passaged by dissociation with Neurocult Chemical Dissociation Kit (Stem Cell Technologies). For immunostaining, NSPCs and HFF cells were plated on #1.5 glass coverslips (Warner Instruments). For live cell TIRFM imaging, mNSPCs cells were plated on #1.5 glass Mat-Tek dishes (Mat-Tek Corporation). Glass substrates were coated with 20 µg/ml laminin (Invitrogen/Life Technologies).

HFF cell culture. Human foreskin Fibroblasts (HFF-1) were purchased from ATCC (ATCC® SCRC-1041™) and cultured in medium consisted of high-glucose Dulbecco's modified Eagle's medium (all reagents from Life Technologies unless otherwise noted), 1 mM sodium pyruvate, 1x MEM-NEAA, 1% Pen/Strep, and 10% heat-inactivated FBS (Omega Scientific). Cells were passaged 1:5 with TrypLE every 4-5 days. For live cell TIRFM imaging, cells were plated on No. 1.5 glass Mat-Tek dishes (Mat-Tek Corporation) coated with 10 µg/ml human fibronectin (Corning).

MEF cell culture. Piezo1 heterozygous null mice (Ranade et al. 2014)were obtained from Jackson Laboratories (Stock No. 026948) and intercrossed to generate a mixture of wildtype, heterozygous, and knockout embryos. The time of the vaginal plug observation was considered E0.5 (embryonic day, 0.5). Dams were sacrificed E10.5, and mouse embryonic fibroblast (MEF) were derived from individual embryos as per Behringer et al. (Behringer et al. 2014). Tissue was mechanically dissociated, and cells were seeded onto plates coated with 0.1% Gelatin (Millipore ES-006-B), and passaged twice before experimentation. Growth medium consisted of DMEM (ThermoFisher, 11960-051), 10% FBS (Omega Scientific, FB-12), 1x GlutaMAX (ThermoFisher, 35050061), 1x Pen-Strep (ThermoFisher, 15140122), and 20 ng/ml PDGF (PeproTech, 100-00AB). Genotyping was performed through Transnetyx, and cells of the same genotype were pooled. Prior to TIRFM imaging, MEFs were dissociated with TrypLE Express (ThermoFisher, 12604013) and 5000 cells were plated onto 14 mm #1.5 glass Mat-Tek dishes coated with 10 µg/ml fibronectin (Fisher Scientific, CB-40008A). MEFs were imaged 2 days after seeding.

Generation of micropatterned square cells. Coverslips with square micropatterns were purchased from Cytoo (https://cytoo.com/, Catalog # CYTOOchips PADO-SQRS). CYTOOchips were coated with fibronectin per manufacturer's instructions and hNSPCs were plated using a density of 1.5 x 10^4 cells/ml per manufacturer's instructions in growth media. For TIRFM Ca^{2+} imaging live cells were imaged 2-5 hours after seeding. For immunofluorescence experiments, cells were fixed with 4% paraformaldehyde in phosphate-buffered saline supplemented with 5 mM $MgCl_2$, 10 mM EGTA, 40 mg/ml sucrose, pH 7.5.

Generation of Piezo1-knockout HFFs by CRISPR/Cas9.

The Piezo1 gene was edited using the D10A nickase mutant of Cas9 (Cas9n) from S. pyogenes to limit

off-target effects (Ran et al. 2013). The Zhang lab design tool:http://crispr.mit.edu/ was used to identify optimal and specific Guide A and Guide B sequences (Hsu et al. 2013). The guide sequences targeting Piezo1 exon 19 were cloned into plasmids with the sgRNA encoding backbone and had either the green fluorescence protein gene, 2A-EGFP (pSpCas9n(BB)-2A-GFP, PX461, Addgene Cat. #48140) or the puromycin resistance gene (pSpCas9n(BB)-2A-Puro (PX462) V2.0, PX462, Addgene Cat. #62987). PX461 and PX462 were a gift from Feng Zhang (Ran et al. 2013). Guide A sequence (GCGTCATCATCGTGTGTAAG) was subcloned into PX461 while Guide B sequence (GCTCAAGGTTGTCAACCCCC) was subcloned into PX462.

Equal amounts of Guide A and Guide B plasmids (5 µg) were co- transfected into HFFs at passage 8 using NHDF Nucleofection® Kit (Neonatal cells protocol, Cat. # VAPD-1001 10) as per kit instructions using Nucleofector® Program U-020. Cells were treated with 5 µg/ml puromycin for 2 days following transfection (conditions in which all untransfected HFF cells die). Surviving cells were examined by fluorescence microscopy which revealed most cells to exhibit green fluorescence indicating that these cells contained both plasmids. Cells were plated to obtain single cells in 96-well plates (100 µl of 5 cells/ml per well) and expanded in 2% O_2 and 5% CO_2 incubator at 37º C. Genetic identification was performed by isolating gDNA from individual HFF clones using DNeasy Blood and Tissue kit (Qiagen) and amplifying the CRISPR/Cas9 targeted exon 19 region by PCR. The PCR products were subcloned into pGCBlue (Lucigen, pGCBlue Cloning and Amplification kit) or pMiniT (NEB PCR cloning kit, Cat. # E1202S) plasmids and sequenced. Sequence analysis of Clone 18-3 revealed out of frame indel modifications on both alleles in exon 19: 18 subclones had a 32 bp deletion with a 1 bp insertion (T), while 17 subclones had a 44 bp deletion.

Wild type: GCGTCATCATCGTGTGTAAGATGCTGTACCAGCTCAAGGTTGTCAACCCCC

ALLELE #1 GCGTC----------TGGTTGTCAACCCCC (32 bp deletion, 1 bp (T) insertion)

ALLELE #2 GCG----------CCCC (44 bp deletion)

HFF clones were imaged in TIRFM assays as described above. As an appropriate control for experiments presented in Fig. 1B, a wildtype clone (9-7) isolated from the above procedure was used. We did not observe any differences in Ca^{2+} flickers in the parent HFF population and the 9-7 WT clone.

Immunofluorescence Staining.

Immunostaining was performed as previously described(Pathak et al. 2014) using the following antibodies: Rabbit anti-RFP (RFP Antibody Pre-adsorbed; Rockland, Cat# 600-401-379), 1:200 (0.95 µg/ml) and mouse anti-paxillin (clone 5H11, Millipore Cat # 05-417), 1:1000, mouse anti-Integrin (IGTB1; clone 2B1, Fisher Scientific cat # MA10690), 1:100. Secondary antibodies used were Goat anti-rabbit Alexa Fluor 555 (Invitrogen Cat# A21428) and Donkey anti-mouse Alexa Fluor 488 (Invitrogen, Cat# A-21202), and Goat anti-Mouse Alexa Fluor 488 (Invitrogen, Cat# A11029) were used at 1:200 (0.01 mg/ml). Nuclei were stained by Hoechst 33342 (Life Technologies) at 4 µg/mL in PBS and actin filaments were stained with Phalloidin conjugated with TRITC (Sigma-Aldrich Catalog #P1951). Samples were mounted with Prolong Diamond anti-fade (Invitrogen cat # p36961).

Imaging

Imaging Piezo1 flickers. Piezo1 flickers were detected using Ca^{2+} imaging by TIRF microscopy. Cells were loaded by incubation with 1-2 µM Cal-520 AM (AAT Bioquest Inc.) in phenol red-free DMEM/F12 (Invitrogen) for 20-30 min at 37 °C, washed three times, and incubated at room temperature for 10–15 min to allow cleavage of the AM ester. Imaging was performed at room temperature in a bath solution comprising 148 mM NaCl, 3 mM KCl, 3 mM $CaCl_2$, 2 mM $MgCl_2$, 8 mM glucose, and 10 mM HEPES (pH adjusted to 7.3 with NaOH, Osmolarity adjusted to 313 mOsm/kg with sucrose). We refer to this solution

as the standard imaging solution below.

For imaging Piezo1 flickers in hNSPCs in Fig. 1 and Fig. 2, movies were acquired at 100 or 200 Hz frame rate on a custom-built Spinning-Spot Shadowless TIRF microscope. Details of construction and comparison to traditional TIRF can be found in Ellefsen et al. 2015(Ellefsen, Dynes, and Parker 2015).

Piezo1 flickers in HFFs (Fig. S1, Fig. S2, Movie M1) were imaged on a motorized Olympus IX83 microscope, equipped with an automated 4-line cellTIRF illuminator and a PLAPO 60x oil immersion objective with a numerical aperture of 1.45. Mat-tek dishes of shRNA-transfected cells loaded with Cal-520 AM were first scanned using an Olympus UPLSAPO 10x objective to identify cells expressing TurboRFP. Spatial coordinates of red fluorescent cells were marked using a programmable stage (Applied Scientific Instruments). Then the objective lens and illumination were switched for TIRF imaging, and previously identified red cells were imaged for Piezo1 flicker activity. Cells were illuminated with a 488 nm laser and images were acquired with a Hamamatsu Flash v4 scientific CMOS camera at 10 ms exposure and a frame rate of 9.54 frames/second.

Imaging Piezo1 flickers and cellular traction forces in the same cell. Fabrication of Förster resonance energy transfer (FRET)-based molecular tension sensors (MTSs) to measure cellular traction forces was performed as previously described(Chang et al. 2016). The MTS is comprised of an elastic spring domain derived from spider silk, which is flanked by a covalently-bound FRET pair, Alexa 546 and Alexa 647. The N-terminus of the sensor possesses a HaloTag domain, while the C-terminal end presents the ninth and tenth type III domains of fibronectin.

Perfusion chambers (Grace Biolabs 622103) were attached to HaloLigand/PEG-functionalized coverslips. The MTS (at 0.03 mM for HFFs and 0.04 mM for hNSPCs) was added to the flow cell and incubated at room temperature for 30 min, washed with PBS twice, and passivated with 0.2% w/v Pluronic F-127 for 5 min. Flow cell channels were washed once with PBS before adding freshly dissociated cells in normal culture media and incubated at 37 °C with 5% CO_2. Cells were typically allowed to spread for 1 h before imaging and not imaged for longer than 5 h after seeding. Cells were loaded with Cal-520 AM Ca^{2+} indicator as described above and imaged in DMEM/F12 medium containing 10% FBS and 3 mM $CaCl_2$.

FRET-based traction force measurements and Piezo1 flicker measurements were performed with TIRFM on an inverted microscope (Nikon TiE) with an Apo TIRF 100x oil objective lens, NA 1.49 (Nikon). The FRET probe was excited with 532 nm (Crystalaser). Emission from Alexa 546 and Alexa 647 was separated using custom-built optics as described previously(Chang et al. 2016; Morimatsu et al. 2015). Donor and acceptor images were focused on the same camera chip. Data were acquired at 5 frames per second with an EMCCD camera (Andor iXon). Following imaging of the FRET force sensor, a motorized filter flip mount (Thor Labs) was used to switch emission filters for imaging Cal-520 Ca^{2+} indicator in the same cell. Cal-520 was excited using a 473 nm (Coherent Obis) laser and imaged at 15.29 ms exposure time.

Effect of pharmacological agents on Piezo1 Ca^{2+} flickers. Yoda1 (Tocris Bioscience), ML-7 (Cayman Chemicals), and Calyculin-A (Cayman Chemicals) were dissolved in anhydrous dimethyl sulfoxide (DMSO) to make stock solutions of 10 mM Yoda1, 10 mM Y-27632, 50 mM ML-7 and 100 µM Calyculin A. Working concentrations used were 2 µM Yoda1, 10 µM Y-27632, 50 µM ML-7 and 10 nM Calyculin A in standard imaging solution (see above for composition). For control measurements, comparable volumes of DMSO were added for each experiment. For experiments requiring 0 mM external Ca^{2+} the imaging solution used was 138 mM NaCl, 1 mM KCl, 5 mM $MgCl_2$, 2 mM EGTA, 8 mM glucose, and 10 mM HEPES, pH 7.3, 313 mOsm/kg. For ML-7 treatment, cells were incubated in HFF Media containing 50 µM ML-7 for 30 minutes at 37 °C, then loaded and imaged with Cal-520 AM in the presence of 50 µM ML-7. For Calyculin A treatment, after control measurements in standard imaging solution, the bath solution was replaced with imaging solution containing 10 nM Calyculin A and cells were imaged after incubation for 1-5 minutes at room temperature. For Yoda1 treatment, after control measurements in standard imaging solution, the bath solution was replaced with 2 µM Yoda1, cells were incubated at room temperature for 10 min and then imaged.

Imaging Piezo1 diffusion with TIRFM. For Piezo1 diffusion studies in Fig. 4B-D, images were acquired on a Nikon N-STORM system built around a Nikon Eclipse Ti microscope. The imaging objective used was a Nikon 100x APO TIRF oil immersion objective (NA 1.49). Images were acquired on an Andor iXon3 electron-multiplying charge-coupled device (EMCCD) camera with an 100 ms exposure time and 160 nm/px in TIRF mode. Cells were continuously illuminated with a 561 nm laser.

Imaging Piezo1 diffusion with lattice light-sheet imaging. Lattice light-sheet imaging for Fig. S3 was performed using a custom built system as described (Ellefsen & Parker, 2018). In brief, a lattice pattern created by a custom graticule was projected through an annular aperture onto the back focal plane of a projection objective (Nikon, 40x NA 0.8 water immersion) to generate an array of Bessel beams creating an effective light sheet with a thickness of ~ 1.2 mm and extent of 50 x 25 mm. A 562 nm laser was used for fluorescence excitation of Piezo-tdTomato, and emitted light was captured by an identical, orthogonal 40x objective lens, passed through a 610 nm long-pass filter, and imaged by an Andor Zyla 4.2 sCMOS camera at a final resolution of 110nm/px.

Confocal imaging. Confocal imaging was performed on a Zeiss Confocal Spinning Disc Confocal Microscope (Zeiss) using a 63X objective with a numerical aperture of 1.40. Image stacks were acquired with 405nm, 488nm, and 561nm lasers, in intervals of 0.3 µm thickness using the AxioVision Rel 4.8 software.

Image analysis

Automated detection of Piezo1 flickers. Piezo1-mediated Ca^{2+} flickers were detected using an improved version of our published algorithm for automated detection of Ca^{2+} signals(Ellefsen et al. 2014). The new algorithm, which runs as a plug-in under the open-source image processing and analysis package Flika (https://github.com/flika-org/flika), uses a clustering algorithm(Rodriguez and Laio 2014) to group super-threshold pixels into calcium events, improving both signal detection and segregation of signals which overlap temporally or spatially.

An F/F_0 movie is generated from the original recording by subtracting the camera black level and dividing each pixel at every frame by its average value across the first ~100 frames. To remove low temporal frequency signal drift, the F/F_0 movie is temporally filtered with a high pass Butterworth filter. To standardize variance across pixels, the value of each pixel is divided by the standard deviation of the values at baseline. The noise in this 'normalized' movie is normally distributed with a mean of 0 and standard deviation of 1.

A threshold is applied to a spatially-filtered version of the 'normalized' movie to generate a binary movie. Each super-threshold pixel in this binary movie is putatively considered part of a flicker. In order to group these pixels together, we modified the clustering algorithm published by Rodriguez and Laio(Rodriguez and Laio 2014). Briefly, a density is assigned to every super-threshold pixel by counting the number of pixels in an user-defined ellipsoid centered around the pixel. Then, for every pixel, the distance to the nearest pixel with a higher density is determined. Pixels that represent the center of clusters will have both a high density and a high distance to a pixel with higher density. The user manually selects pixels exceeding a density and distance threshold as cluster centers. The algorithm then assigns every other pixel to a cluster center pixel recursively, by finding the cluster of the nearest pixel of higher density. Once all pixels have been clustered, clusters below a user-defined size are removed.

After flickers have been identified by the clustering algorithm, the subpixel centroid of the signal is found by averaging each pixel in the 'normalized' movie over the flicker duration, and fitting a 2D Gaussian function to this average image. The peak amplitude, temporal dynamics, and frequency of signals at specific sites can be quantified, and the resulting data can be exported as Excel or csv files.

This algorithm is implemented in the puff_detect plugin for the image analysis software Flika, downloadable at https://github.com/kyleellefsen/detect_puffs. Both the puff_detect plugin and flika are open source software written in the Python programming language. Instructions for installation and use of the algorithm can be found at http://flika-org.github.io/.

Generation of cellular force maps. Analysis of FRET signals from the MTS was performed following the methodology from Morimatsu & Mekhdjian et al., Nano Letters 2015. Briefly, FRET index maps were generated by dividing the acceptor intensity A (background subtracted) by the sum of the acceptor and donor (D) intensities (also background subtracted): $FRET_i = A / (A + D)$. FRET index maps can be converted to FRET efficiency maps to extract quantitative values for force from the FRET efficiency to force calibration curve. FRET index is converted to FRET efficiency using the following equation:

$$E = (FRET_i)/(\alpha (\gamma\text{-}FRET_i \gamma + FRET_i))$$

Where E is the FRET efficiency, $FRET_i$ is the FRET index, α is the fraction of donor-labeled sensors that have an acceptor, and γ is a factor that accounts for differences in donor and acceptor quantum yield. Both α and γ are experimentally determined (Morimatsu et al., Nano Letters 2015). The FRET efficiency is converted to force using a phenomenological fit (Chang et al., ACS Nano 2016) to the FRET-force response of the $(GPGGA)_8$ linker (Grashoff et al., Nature 2010).

Calculation of distance from Piezo1 flicker localization to nearest force-producing region. Force-generating regions were determined by blurring the force maps with a Gaussian filter. Regions in which the pixel intensity was below 75% of maximum intensity were considered force generating. Distances from each flicker centroid to the nearest force generating region were measured. To calculate the average distance to the nearest force generating region in each cell, the outline of each cell was manually traced, 1000 points were randomly selected inside this outline, and the distance to the nearest force generating region was measured.

Piezo1 particle tracking. TIRFM image stacks were processed in order to determine the location of Piezo1-tdTomato puncta in each frame. Each frame was spatially bandpass filtered by taking the difference of Gaussians, an image processing algorithm that enhances a band of spatial frequencies--in this case, around the size of the particles. The spatially filtered movie was then thresholded using a manually determined threshold, yielding a binary movie. Spatially contiguous pixels above threshold were grouped together and considered a single particle. The centroid for each particle was determined by fitting a 2D Gaussian function to each particle, yielding a centroid with subpixel precision. The initial x, y values for the fit were set to be the center of mass of the binary pixels in the particle. Any localizations within consecutive frames that were within three pixels of each other were assumed to arise from the same particle. These localizations were linked over time to generate particle tracks.

Piezo1-tdTomato puncta in single mNSPCs and in neurospheres imaged with lattice-lightsheet microscopy were tracked using the 2D/3D particle tracker which is part of the MosaicSuite ImageJ plugin(Sbalzarini and Koumoutsakos 2005). Only particles larger than a radius of 7 pixels were considered.

Data analysis and statistical testing

OriginPro 2018 (OriginLab Corporation) was used for statistical analysis and generating plots. P values and statistical tests used are indicated in figure legends. A two-sample t-test was used where data were modeled by a normal distribution and the non-parametric Kolmogorov-Smirnov test was used in the case of non-normal distributions.

References

Behringer, Richard, Marina Gertsenstein, Kristina Vintersten Nagy, and Andras Nagy. 2014. Manipulating the Mouse Embryo: A Laboratory Manual. Cold Spring Harbor Laboratory Press.

Chang, Alice C., Armen H. Mekhdjian, Masatoshi Morimatsu, Aleksandra Kirillovna Denisin, Beth L. Pruitt, and Alexander R. Dunn. 2016. “Single Molecule Force Measurements in Living Cells Reveal a Minimally Tensioned Integrin State.” ACS Nano 10 (12): 10745–52.

Ellefsen, Kyle L., Joseph L. Dynes, and Ian Parker. 2015. “Spinning-Spot Shadowless TIRF Microscopy.” PloS One 10 (8): e0136055.

Ellefsen, Kyle L., Brett Settle, Ian Parker, and Ian F. Smith. 2014. “An Algorithm for Automated Detection, Localization and Measurement of Local Calcium Signals from Camera-Based Imaging.” Cell Calcium

56 (3): 147–56.

Hsu, Patrick D., David A. Scott, Joshua A. Weinstein, F. Ann Ran, Silvana Konermann, Vineeta Agarwala, Yinqing Li, et al. 2013. “DNA Targeting Specificity of RNA-Guided Cas9 Nucleases.” Nature Biotechnology 31 (9): 827–32.

Morimatsu, Masatoshi, Armen H. Mekhdjian, Alice C. Chang, Steven J. Tan, and Alexander R. Dunn. 2015. “Visualizing the Interior Architecture of Focal Adhesions with High-Resolution Traction Maps.” Nano Letters 15 (4): 2220–28.

Nourse, J. L., J. L. Prieto, A. R. Dickson, J. Lu, M. M. Pathak, F. Tombola, M. Demetriou, A. P. Lee, and L. A. Flanagan. 2014. “Membrane Biophysics Define Neuron and Astrocyte Progenitors in the Neural Lineage.” Stem Cells 32 (3): 706–16.

Pathak, Medha M., Jamison L. Nourse, Truc Tran, Jennifer Hwe, Janahan Arulmoli, Dai Trang T. Le, Elena Bernardis, Lisa A. Flanagan, and Francesco Tombola. 2014. “Stretch-Activated Ion Channel Piezo1 Directs Lineage Choice in Human Neural Stem Cells.” Proceedings of the National Academy of Sciences of the United States of America 111 (45): 16148–53.

Ranade, Sanjeev S., Zhaozhu Qiu, Seung-Hyun Woo, Sung Sik Hur, Swetha E. Murthy, Stuart M. Cahalan, Jie Xu, et al. 2014. “Piezo1, a Mechanically Activated Ion Channel, Is Required for Vascular Development in Mice.” Proceedings of the National Academy of Sciences of the United States of America 111 (28): 10347–52.

Ran, F. Ann, Patrick D. Hsu, Jason Wright, Vineeta Agarwala, David A. Scott, and Feng Zhang. 2013. “Genome Engineering Using the CRISPR-Cas9 System.” Nature Protocols 8 (11): 2281–2308.

Rodriguez, Alex, and Alessandro Laio. 2014. “Clustering by Fast Search and Find of Density Peaks.” Science 344 (6191): 1492–96.

Sbalzarini, I. F., and P. Koumoutsakos. 2005. “Feature Point Tracking and Trajectory Analysis for Video Imaging in Cell Biology.” Journal of Structural Biology 151 (2): 182–95.